For the convenience of the reader, we are **reprinting** below (in the print journal only) the text of Phys. Rev. B **70**, 195408 (2004), to which the Publisher's Note printed in this issue [209901(E)] refers.

Observation of Fano resonances in single-wall carbon nanotubes

B. Babić and C. Schönenberger*
Institut für Physik, Universität Basel, Klingelbergstrasse 82, CH-4056 Basel, Switzerland
(Received 23 June 2004; published 10 November 2004; publisher error corrected 9 May 2005)

We have explored the low-temperature linear and nonlinear electrical conductance G of metallic carbon nanotubes (CNT's), which were grown by the chemical-vapor deposition method. The high transparency of the contacts allows to study these two-terminal devices in the high conductance regime. We observe the expected four-fold shell pattern together with Kondo physics at intermediate transparency $G \lesssim 2e^2/h$ and a transition to the open regime in which the maximum conductance is doubled and bound by $G_{\max}=4e^2/h$. In the high-G regime, at the transition from a quantum dot to a weak link, the CNT levels are strongly broadened. Nonetheless, sharp resonances appear superimposed on the background which varies slowly with gate voltage. The resonances are identified by their lineshape as Fano resonances. The origin of Fano resonances is discussed along the modeling.

DOI: 10.1103/PhysRevB.70.195408 PACS number(s): 73.63.Fg, 73.63.Kv, 81.07.De, 85.35.Ds

I. INTRODUCTION

The Fano resonance (FR) is a universal physical phenomenon which has historically been discovered as asymmetric line profiles in spectra of rare gases.[1] This effect has successfully been interpreted by Fano in terms of the interference between an autoionized state and the continuum.[2] FR's have, for example, been observed in the spectroscopy of atoms and molecules,[1] in electron, neutron, and Raman scattering.[3–5]

Generally speaking, the interference of a resonant state (the resonant channel) with a continuum (the nonresonant channel) gives rise to Fano line shapes. An illustration is shown in Fig. 1(a). This phenomenon can also naturally arise in coherent electrical transport through nanostructures. Indeed, Fano line shapes were observed in the differential electrical conductance dI/dV vs V, while tunneling with a scanning tunneling microscope through an impurity atom on a metal surface.[6,7] The first observation of FR's in mesoscopic devices has been reported by Göres *et al.* in a single-electron transistor fabricated into a gated two-dimensional electron gas.[8] Thereafter, FR's have been found in several studies of charge transport through similarly fabricated "two-dimensional" quantum dots, both for single quantum dots and quantum dots embedded into an Aharonov-Bohm ring.[9–12] Recently, several groups have reported the observation of FR's in multiwall carbon nanotubes (MWNT's). Kim *et al.*[13] observed the FR on crossed MWNT's, while Yi *et al.*[14] reported on FR's measured in MWNT bundles. Furthermore, Fano resonances have been measured on an individual MWNT.[15] However, similar observations have not yet been reported for single-wall carbon nanotubes (SWNT's).

Following the notion of Fano,[2] the energy-dependent conductance $G(E)$ of a Fano resonance observed in a transport measurement can be described in the following form:[8]

$$G(\epsilon) = G_{\text{nonres}} + G_{\text{res}}\frac{(\epsilon+q)^2}{\epsilon^2+1}, \qquad (1)$$

where G_{nonres} and G_{res} denote incoherent and coherent contributions to the conductance. The detuning of the energy E from the center of the resonance E_0 is described by the dimensionless parameter $\epsilon \equiv 2(E-E_0)/\Gamma$, where Γ denotes the width of the resonant state. q is the so-called asymmetry parameter. Its magnitude is proportional to the ratio of the transmission amplitudes of the resonant and nonresonant channel. In the original Fano work,[16] q was introduced as a real parameter, in general however, it must be treated as a complex quantity.[17] In the limit $q \to \infty$, resonant transmission dominates which leads to symmetric Breit-Wigner resonances, see Fig. 1(b). In the opposite limit $q \to 0$, the resonant transmission appears as an antiresonance, i.e., a symmetric dip. In all other cases, e.g., $q=1$, asymmetric line shapes are obtained. These asymmetric line shapes are characteristic for the Fano effect and that is why one refers to them as Fano line shapes.

Since the Fano resonance is the result of an interference effect, its line shape is sensitive to the phase difference between the two transmission pathways. Fano resonances can therefore provide essential information on dephasing in mesoscopic systems.[9–11,17] In this respect it has the same power as all other two-path interference experiments, for example the Aharonov-Bohm experiment.[18]

Here we report on the observation of Fano resonances in electrical transport measurements on SWNT's. In contrast to previous studies, which were focussed on two-dimensional quantum dots, SWNT's can be classified as one-dimensional quantum dots. MWNT's are different, because it has been shown that several subbands are in general occupied,[19,20] giving rise to the possibility that more than one quantum dot state may participate in transport.

II. EXPERIMENTAL

Single wall carbon nanotubes (SWNT's) have been grown from patterned catalyst islands by the chemical vapor deposition (CVD) method on Si/SiO_2 substrates.[21] The degenerately doped silicon, terminated by a 400 nm thick SiO_2 layer, is used as a back-gate to modulate the electrochemical potential of the SWNT electrically contacted with a source and drain terminal. Electrical contacts to individual tubes are patterned by electron-beam lithography. Once the samples are

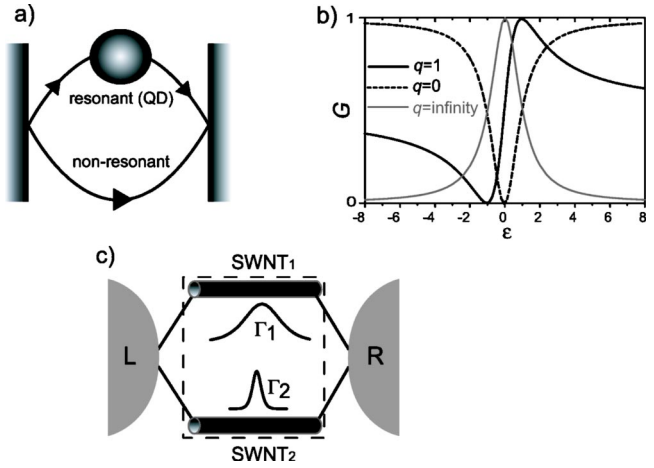

FIG. 1. (a) Schematic view of a Fano system consists of a resonant channel through, e.g., a quantum dot (QD), and a nonresonant channels. (b) Normalized Fano line shapes calculated from Eq. (1) for several asymmetry q parameters. (c) A scheme of two SWNT's connected to the left (L) and right (R) leads. Due to different coupling strength the zero-dimensional states of each SWNT acquires a different width expressed by $\Gamma_{1,2}$. The two interfering channels may be due to two "individual" SWNT's of a bundle or may represent the two transport channels of one and the same SWNT.

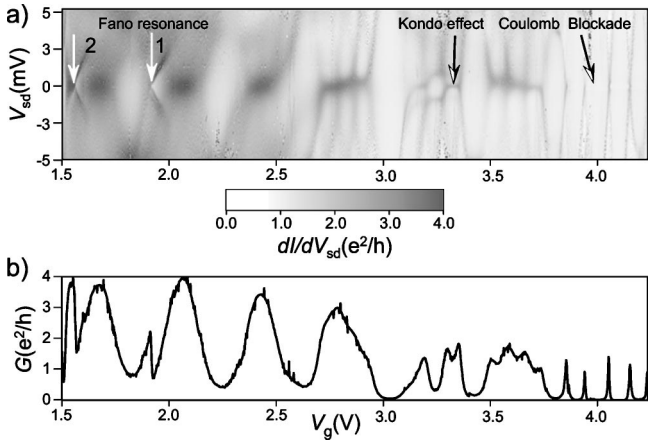

FIG. 2. (a) Grey-scale representation of the differential conductance (dI/dV_{sd}) versus bias (V_{sd}) and gate voltage (V_g) and (b), the corresponding linear response conductance versus gate voltage. Due to the strong dependence of the tunneling coupling to the leads on gate voltage, several physical phenomena are observed together. These are from right to left: Coulomb blockade, the Kondo effect and Fano resonances, corresponding to regimes of low, intermediate and high tunneling coupling. Note, that the conductance dramatically increases for $V_g \lesssim 3$ V reaching a maximum value of $G \approx 4e^2/h$ as expected for an ideal metallic SWNT.

made, semiconducting and metallic SWNT's are distinguished by the dependence of their electrical conductance G on the gate voltage V_g measured at room temperature.[22] Here, we focus on measurements performed on metallic SWNT's with relatively low-Ohmic contacts. We found independently of the work by Javey *et al.*[23] that palladium makes excellent contacts to SWNT's. There is no need for an additional post-growth treatment (e.g., annealing).[22,24] Most of the samples show two-terminal conductances of $G > e^2/h$ which is essential for the studies discussed below.

The electrical characterization of the devices has been performed at 300 mK in a ^{3}He system. We measure the electrical current I with a low noise current to voltage amplifier as a function of source-drain and gate (V_g) voltage and determine the differential conductance $G_d := dI/dV_{sd}$ numerically. Finally, the collected data $G_d(V_{sd}, V_g)$ is represented in a two-dimensional grey-scale representation in which the grey-scale corresponds to the magnitude of G_d. The linear-response conductance $G := I/V_{sd}$ with $V_{sd} \to 0$ is measured at a small but finite source-drain voltage of 40 μV.

III. OBSERVATION OF FANO RESONANCES IN SWNT's

Figure 2(a) shows the differential conductance in the form of a grey-scale plot of a single nanotube device for a relatively large gate voltage range. The corresponding dependence of the linear response conductance on the gate voltage V_g is displayed in Fig. 2(b). This measurement is remarkable in that the tunneling coupling between the nanotube and the contacts must vary substantially, from weak coupling at large gate voltage to very strong coupling at low gate voltage. For large positive gate voltages ($V_g \gtrsim 4$ V) a clear Coulomb blockade pattern of low-conductance regions is observed which is characteristic for weak coupling. As the gate voltage is reduced higher-order tunneling processes (so called co-tunneling) start to dominant, forming high conductance Kondo resonances around zero source-drain voltage,[25–27] within the well known fourfold shell pattern generic for high-quality carbon nanotubes.[28–30] Reducing the gate voltage even further and hence increasing the transparency to the contact blurs the Coulomb blockade diamonds. This signals the transition from a quantum dot to an open wire, which occurs if the lifetime broadening Γ approaches the level spacing δE, which in this device is of the same order as the charging energy $U_C \sim 5$ meV. In the limit $\Gamma \gg U_C$, interaction can be neglected. The overall transparency is then expected to approaches unity, which for a single nanotube with four channels relates to an upper bound in conductance of $G = 4e^2/h$. Because of residual backscattering at the contacts, a weak periodic conductance modulation with gate voltage is expected. This has been observed recently in SWNT's at a mean transparency of $T = 0.7$ and was termed the Fabry-Perot interference effect.[31] The mean net transparency in our device approaches $T = 0.5$ for the lowest gate voltage.

Instead of a smooth continuation from the cotunneling to the Fabry-Perot regime, sharp resonances appear below $V_g = 2$ V. The two resonances visible in Fig. 2(a). (labeled 1 and 2) are identified by their asymmetric line shapes as Fano resonances. To show this, the measured gate dependence of the linear conductance for the two resonances is magnified in Fig. 3 (symbols) and shown together with fits (solid curves) of Eq. 1 using the appropriate factor to convert gate voltage into energy (i.e., $eC_g/C_\Sigma = 0.025 \pm 0.05$). Here, we compare two parameters which are obtained from the fitting procedure, Γ and q. Γ equals ≈ 0.25 and ≈ 0.5 meV for resonance

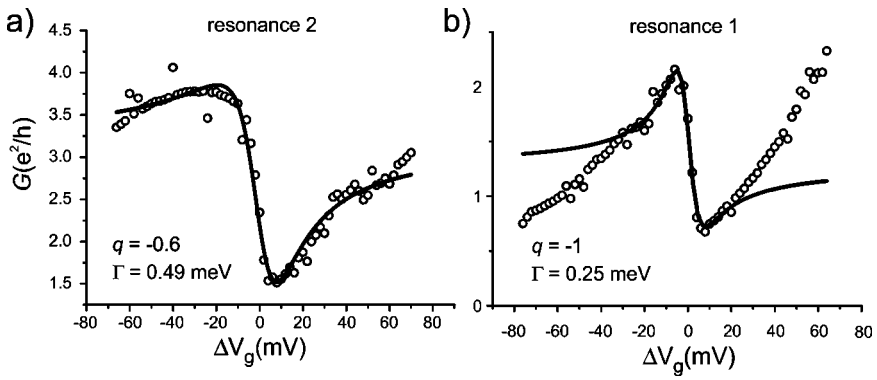

FIG. 3. Comparison of the measured (symbols) linear response conductance G for the resonances labeled 2 (a) and 1 (b) in Fig. 2(a) with the Fano formula (1) (solid curves). $\Delta V_g := V_g - V_g^0$, where V_g^0 denotes the gate voltage at the center of the resonance: $V_g^0 = 1.9$, 1.54 V for resonance 1 and 2. The extracted values from the fits to the Fano equation are $q = -1.0 \pm 0.16$, -0.63 ± 0.05 and $\Gamma = 0.25 \pm 0.05$, 0.49 ± 0.08 meV for resonances 1 and 2, respectively.

1 and 2, respectively. For comparison we have also extracted Γ in the cotunneling regime and found values ~ 2 meV. Hence, the width of the two new features is substantially smaller than the width of the broadened nanotube levels. This difference gets even larger if we take into account that Γ grows further if one proceed from the cotunneling regime at $V_g \sim 3.5$ V to the "open" regime at $V_g \sim 2$ V. Both fits yield an asymmetry parameter q close to unity, i.e., $q = -1$ and $q = -0.65$ for resonance 1 and 2, respectively. An asymmetry parameter with a magnitude close to 1 corresponds to asymmetric line shapes that are characteristic for Fano resonances, see Fig. 1(b). We note that both resonances have comparable q parameters of order 1 and that the change in conductance is for both cases large and of order e^2/h. The Fano fit is very good for resonance 2 and it is reasonable for resonance 1. In the latter case the deviations are getting appreciable away from the resonance. Referring to the grey-scale plot in Fig. 2(a) we see that this resonance is superimposed on a low-conductance and strongly blurred Coulomb blockade diamond. The assumption of the Fano description that the background contributes to the interference with a constant non-energy-dependent term is only approximately valid here. These two resonances will be analyzed further below.

The emergence of Fano resonances in single-wall carbon nanotubes is exciting and we have therefore measured this sample again, now lowering the gate voltage even further. This measurement is shown in Fig. 4. A complex pattern of resonances appears (arrows). We find resonances, antiresonances, and asymmetric Fano lines shapes. All features resemble Fano resonances for different q values. Although the overall pattern looks quite irregular at first sight, regular structures can be identified: In the first place, one can identify "inverted" Coulomb blockade diamonds (indicated with white arrows). Secondly, all resonances have slopes which are quite comparable to the one in the Coulomb blockade regime suggesting that the nanotube itself is the source of the resonant state. The latter is also suggested by the fact that in the whole gate voltage range the differential conductance reaches the maximum conductance for a single SWNT of $4e^2/h$, but never exceeds it.

IV. DISCUSSION AND MODELING

The origin of the interfering paths, necessary for the Fano effect, in a single quantum dot is often unclear.[8,32] One usually refers to the following picture: the non-resonant channel can be seen as the direct transmission between the open source and open drain contacts, while the weakly coupled resonant state corresponds to a bound state, localized in the interior of the quantum dot.[17]

In carbon nanotubes the first account of Fano resonances have been reported for crossed MWNT's.[13] Because these authors have not observed similar resonances in single tubes, they assigned the origin of the Fano resonance to the particular geometry of two crossed tubes. In further accounts of Fano resonances in MWNT's, the origin has been assigned to either an additional carbon nanotube[14] acting as the nonresonant background or to defects in the nanotube.[15]

Our experiment is the first for single-walled carbon nanotubes (SWNT's) and the origin is puzzling as well. We point out, that an individual SWNT contains two transport channels (not counting spin), leading to the fourfold shell pattern of CNT quantum dots.[28–30] In principle, this is enough for interference to occur. Assume that the two nearly degenerate eigenstates are coupled with different strength to the source

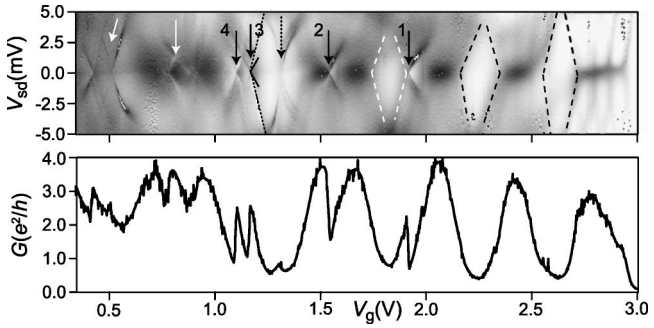

FIG. 4. (a) Differential conductance (dI/dV_{sd}) versus bias voltage (V_{sd}) and gate voltage (V_g). Dark correspond to high (maximum $= 4e^2/h$) and white to low conductance. Fano resonances are indicated with the arrows. (b) Corresponding linear response conductance G.

and drain contacts, one with a large coupling and the other with a weak one. Then, there is a broad and a narrow channel that can interfere and give rise to Fano resonances. This is schematically shown in Fig. 1(c), where $SWNT_1$ and $SWNT_2$ refer to the two orbital channels. However, we emphasize that this picture is too simple for the following reason: The appearance of Kondo resonances with similar Kondo temperatures at intermediate gate voltage for each orbital state proves that they are both coupled strongly to the contacts. It is quite unlikely that the lifetime broadening of one state increases while the other decreases by lowering the gate voltage. Hence, we have to explain the emergence of sharp Fano resonances based on two (nearly) degenerate states which are both strongly coupled to the contacts and have therefore both a large lifetime broadening.

This problem has recently been studied theoretically in the limit of vanishing interaction.[33] Two quantum dot states are coupled to the reservoirs with varying coupling parameters. The calculation shows that even for *similar* coupling strengths the two-dot ground state consists of a narrow and a wide orbital. This is the result of hybridization leading to a symmetric bonding and an asymmetric antibonding state. The latter has a node at the contacts resulting in weak coupling to the leads and therefore a small effective width Γ. If all coupling terms were exactly the same, the life time of the antibonding states would become infinite large. This never happens in practice, so that one can expect intrinsic Fano resonances in SWNT's. This FR was termed "ghost" FR by Ladrón *et al.*[33] This is certainly the most attractive scenario. However, it is obvious that Fano resonances can also occur "extrinsically" for two separate individual SWNT's, provided they are geometrically located within the phase-coherence length. Otherwise, a pure superposition of two individual conductance patterns are expected and not an interference effect. The problem of the interference between two quantum dot states has recently also been addressed using the scattering-(S)-matrix approach.[34,35] These authors also derive the correspondence between the Green's function and S-matrix approach for this problem.

In the case of intrinsic Fano resonances (FR's) the regular periodic pattern, which is evident in our measurement in the Coulomb blockade and cotunneling regime, see Fig. 3(a), should evolve into a periodic pattern of FR's at higher tunneling coupling. Although this looks promising in Fig. 3(a), the FR pattern in Fig. 4(a) is not as periodic as one might expect. This is evidence in favor of extrinsic FR's. On the other hand, the measured conductance is always bound by $4e^2/h$, which is the maximum possible for a single tube. If two different tubes interfere one would expect conductance values exceeding $4e^2/h$ for certain gate voltages, which is not observed. This is evidence in favor of intrinsic FR's. In the following we analyze the observed FR's in greater detail.

Because we have measured both the gate and bias dependence we can extend our analysis of the Fano resonances further and try to fit the differential conductance in the vicinity of the resonance. Below, we will do this for the two resonances 1 and 2. We model the problem as two interfering channels in the Landauer-Büttiker formalism.[36] The transmission amplitude through the resonant channel is described by $t_r=\sqrt{T_r}i/(\epsilon+i)$, where $\epsilon=2(E-E_0)/\Gamma$. The square modulus of this function corresponds to a simple Lorenzian. The transmission amplitude for the nonresonant channel is a constant $t_n=\sqrt{T_n}e^{i\phi}$, where the phase ϕ has been introduced. Assuming spin degeneracy, the conductance at zero temperature is given by $G(\epsilon)=2e^2/h\cdot T_t(\epsilon)$ with the total transmission probability $T_t=|t_r+t_n|^2$. We obtain for T_t

$$T_t = T_n + \frac{1}{1+\epsilon^2}\{T_r + 2\sqrt{T_r T_n}[\cos(\phi) + \epsilon \sin(\phi)]\}. \quad (2)$$

The differential conductance can then be obtained from

$$\frac{\partial I}{\partial V_{sd}} = e^2/h\{T_t(eV_{sd}/2 - \alpha V_g) + T_t(-eV_{sd}/2 - \alpha V_g)\}, \quad (3)$$

where $\alpha := C_g/C_\Sigma$ denotes the gate-coupling strength as before.

We first discuss the symmetry of Eq. (3) and the fitting procedure. The transmission amplitudes through the resonant and nonresonant channel are chosen such that the linear conductance is a Lorenzian for $\phi=0$, whereas it has a Fano line shape ($q=\pm 1$) for $\phi=\pm\pi/2$. Far from the resonance ($\epsilon \rightarrow \infty$) the conductance asymptotically approaches the value of $2e^2/h\cdot T_n$. For $\phi=\pm\pi/2$, the total transmission probability is $T_t=(T_n+T_r)$ at resonance. Note, that the dI/dV_{sd} vs V_{sd} characteristic will not have mirror symmetry in general for positive and negative gate voltages measured relative to the center of the resonance.

The following fitting procedure has been adopted: First, we fit the gate dependence of the linear conductance by changing the phase. Then, the dI/dV_{sd} curves vs V_{sd} are fitted for specific gate voltages close to the resonance. The phase is fixed, whereas T_n, T_r, α, and Γ are free parameters. Thereafter, the gate dependance is plotted again using the average parameters from the fits found from the nonlinear regime. These average parameters are used to calculate the grey-scale plots.

For both resonances this procedure yields a phase close to $\pi/2$ which agrees reasonably with the asymmetry parameter of $q\approx -1$ deduced before. The fitting has been preformed for four Fano resonances indicated with white arrows in Fig. 4(a), but we present only the results for resonances 1 and 2. We start with resonance 2, which is a particularly nice example. Figure 5(a) shows the gate dependence and Fig. 5(b), the bias dependence for four different gate voltages. The solid curve in Fig. 5(a) corresponds to the fit obtained from the linear conductance, whereas the dashed one shows the resonance using the average parameters deduced from the bias dependence. We find for Γ values of 0.25–0.3 meV in good agreement to the values deduced before and a consistent gate-coupling parameter of $\alpha=0.02$. The different values for T_n and T_r are plotted in Fig. 5(c). The spread of $\approx\pm 0.15$ can be seen as a measure of the accuracy of this procedure. Up to this error $T_n=1.3$ and $T_r=0.3$. The average parameters are used to calculate the dI/dV_{sd} grey-scale plot, which is shown together with the measurement in Figs. 5(d) and 5(e). A reasonable agreement is found. The model clearly captures the main features and accounts for the correct energy scales.

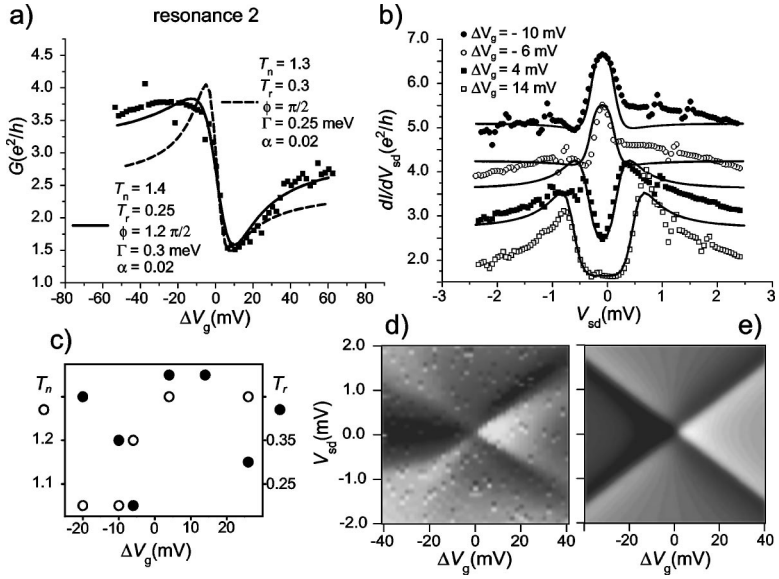

FIG. 5. Comparison between the measured differential conductance of the Fano resonance 2 [see Fig. 4(a)] and fits to Eq. (3). In (a) the dashed curve represents the best fit taking into account only the linear response conductance, whereas the solid curve is calculated from average parameters deduced by fitting the nonlinear differential conductance dI/dV_{sd} vs V_{sd} for a set of gate voltages, shown in (b). The curves are vertically offset by e^2/h for clarity. For (a) the whole set of parameters are given in the figure, whereas we only represent the deduced transmission probabilities for the nonresonant T_n (open circle) and resonant T_r (full circle) channel of part (b) in (c). The calculated differential conductance (e) is compared with the measured one (d). The parameters are $T_n=1.3$, $T_r=0.3$, $\Gamma=0.25$ meV, $\phi=\pi/2$, and $\alpha=0.02$.

The transmission probability of the resonant channel of $T_r=0.3$ relates to a conductance of $0.6e^2/h$, which is quite a substantial value.

We now turn to resonance 1. As we have pointed out before, the agreement is less good here. This is due to the underlying blurred Coulomb blockade structure, which results in a sizable suppression of the conductance on one side of the resonance (left side), see Fig. 4(a). The result of the same procedure that led to Fig. 5 is shown in Fig. 6 for resonance 1. Figure 6(a) displays the gate dependence of the linear conductance. The solid curve corresponds to the fit of the linear conductance vs gate voltage, whereas the dashed curve has been calculated from the average parameters deduced from dI/dV_{sd} vs V_{sd}. Because of the mentioned suppression for $\Delta V_g<0$, the differential conductance has only been fitted in the nonlinear regime for three positive ΔV_g. This is shown in Fig. 6(b), where we see that the fits match (apart from the asymmetry) the measurements quite well. Due to the strongly varying background a sizeable disagreement appears between the two fits in Fig. 6(a). However, we think that this can be fully accounted for, by the background. The obtained parameters ϕ, α, and Γ compare very well with the ones deduced before in Fig. 3(b): $\phi=\pi/2$, $\alpha=0.02$, and $\Gamma=0.2$ meV. Not surprisingly the two fitting procedures

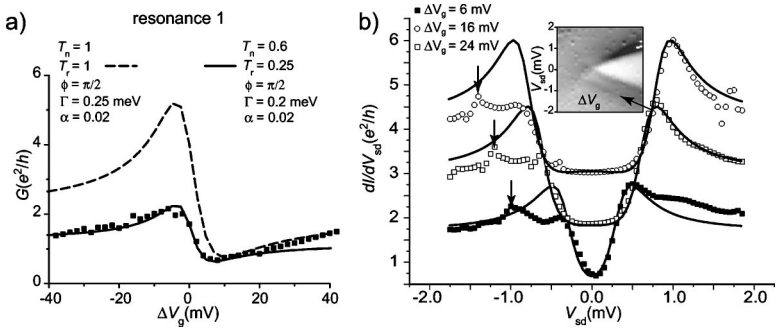

FIG. 6. Comparison between the measured differential conductance of the Fano resonance 1 [see Fig. 4(a)] and fits to Eq. (3). In (a) the solid curve represents the best fit taking into account only the linear response conductance, whereas the dashed curve is calculated from average parameters deduced by fitting the nonlinear differential conductance dI/dV_{sd} vs V_{sd} for a set of (only) positive gate voltages, shown in (b). The curves are vertically offset by e^2/h for clarity. For (a) the whole set of parameters are given in the figure, whereas the parameters for the three fits in (b) are ■: $T_n=0.85$, $T_r=0.9$, $\Gamma=0.25$ meV, $\phi=\pi/2$, and $\alpha=0.027$; □: $T_n=1$, $T_r=1.2$, $\Gamma=0.25$ meV, $\phi=\pi/2$, and $\alpha=0.02$; ○: $T_n=1.1$, $T_r=1.4$, $\Gamma=0.25$ meV, $\phi=\pi/2$, and $\alpha=0.017$. The observed asymmetry in bias voltage originates from different coupling of the resonant states to the leads. The inset in (b) shows the measured differential conductance. An excited state is visible for $V_{sd}<0$, both in the greyscale plot and the $dI/dV_{sd}(V_{sd})$ (arrows).

yield somewhat different values for T_r and T_n. $T_n \approx 1$ and $T_r \approx 1$ in one former and $T_n \approx 0.6$ and $T_r \approx 0.25$ in the latter case.

Important for the following is the observation of an excitation line which appears at negative bias voltage in the measurement and is visible in Fig. 6(b) (arrows), as well as in the grey-scale plot (inset). If we stick to the assumption that the cause of the Fano resonances is intrinsic, the deduced excitation energy of $\delta E = 0.6 \pm 0.1$ meV should then correspond to the level spacing of this nanotube. We immediately see, however, that this value is much smaller than the measured level spacing of $\delta E \approx 5$ meV in this tube, which agrees very well with the particle in a box model assuming spin and orbital degeneracy for a nanotube of length 300 nm, corresponding to the contact separation. If, on the other hand, the FR is extrinsic the resonant channel should correspond to a nanotube with an effective length of as much as $L = 2.8$ μm. This appears to be impossible, since the electrodes are spaced by only 300 nm. However, already in early work on carbon nanotubes (CNT's) two types of characteristics have been found:[37] Contacting tubes by evaporating metals over the tubes yielded "end-contacted" CNT's,[38] whereas CNT's lying on metal electrodes usually displayed a weaker coupling to the contacts and yielded "bulk-contacted" tubes.[39,40] Moreover, the single electron level spacing δE was found to agree with the contact separation from edge to edge in the first case, whereas the whole CNT's appeared to contribute, as apparent from small values of δE in the latter case. The states leading to Fano resonances in our measurements are also much weaker coupled to the leads. This is seen in the relative small Γ values deduced from the Fano resonances. Hence, the underlying resonant channel may very well be a weakly coupled SWNT which resides in one and the same bundle. This model may be regarded a likely scenario because bundling in nanotubes is an ubiquitous phenomenon. It is strong in arc-discharge and laser-evaporated tubes, but it also occurs in CVD-grown CNT's which are considered here.[22,41] We stress, however, that there is no proof that the excitation line corresponds to the level spacing, which we have assumed before. There are also electronic excitation with lower energies possible in carbon nanotubes. For example, at half filling (one electron on each orbital) the exchange energy and level mismatch yield smaller energy scales.[30] Moreover, as we have emphasized before already, if two tubes would contribute to transport, the maximum conductance is not expected to be found to $4e^2/h$.

We next compare the gate-coupling parameter for the Fano resonance (FR) and the cotunneling regime. For the former (Fano resonances labeled 1 and 2) we have obtained $\alpha = 0.02 \pm 0.005$, whereas $\alpha = 0.08 \pm 0.01$ for the latter. This is a significant difference amounting to a factor of 4. This difference is in favor of two tubes, one in effect short and the other long as we explain now. Assume that there are indeed two tubes contributing to the conductance in a small bundle. The gate capacitance C_g can be assumed to be roughly equal, while the capacitances to the leads should be strongly different. The weakly coupled tube, which electrically appears to be much longer than the contact separation, should have much larger source and drain capacitances. The four-times smaller α relates into a four-times larger total capacitance, and hence, into a four-times smaller charging energy. The cotunneling regime of the dominant tube yields $U_C = 5.3$ meV, so that the weakly coupled tube should have a charging energy of $U_C \approx 1.3$ meV. Together with the level spacing of $\delta E \approx 0.6$ meV (assuming that this value does correspond to the level spacing) yields an addition energy of $\Delta E \approx 1.9$ meV. This relatively small addition energy may explain the structure of the Fano resonances at $V_g \approx 1.2, 0.8$ V which are shaped in a diamondlike pattern with an energy scale corresponding to the reduced addition energy, see Fig. 4(a). However, at even smaller gate voltage of $V_g \approx 0.5$ V another "Fano-diamond" appears with obviously a larger addition energy and with a gate-coupling parameter that agrees with the cotunneling regime. Hence, the interfering tube either evolves with increasing tunneling coupling from a weakly coupled "long" tube to a stronger coupled end-contacted one, or part of the observed Fano resonances are intrinsic.

With regard to the phases, which were obtained by fitting resonance 1 and 2, we mention that there is nothing peculiar about the value of $\phi = \pi/2$. The same fitting procedure has also been performed for Fano resonances (FR's) labeled in Fig. 4(a) with 3 and 4 (not shown). Here we obtain the following parameters: $T_n = 0.8$, $T_r = 0.2$, and $\Gamma = 0.23$ meV for FR 3 and $T_n = 0.73$, $T_r = 0.2$, and $\Gamma = 0.23$ meV for FR 4, while the phase is now negative amounting to $\phi = -\pi/2$. $\alpha = 0.02$ is consistent with the previous value and the same for both resonances. In addition, if we go further out to even smaller gate voltages other phase values appear.

Finally, we briefly address the evolution of the Fano resonances (FR's) at larger source-drain voltage V_{sd}. We observe that most of the resonances vanish at $|V_{sd}| \gtrsim 2.5$ meV. This can easily be understood by noting that additional transport channels open up if $V_{sd} > \delta E$. In particular if $V_{sd} > \Delta E \approx 2$ meV the resonant channel can involve excitations even for different charge states. Because different phases are likely, the Fano resonance is smeared out. A peculiar FR is observed at $V_g \approx 1.3$ V in Fig. 4(a) (dashed arrow). This resonance starts with a large gate-coupling α around zero source-drain voltage V_{sd} and evolves into a smaller coupling parameter α for larger V_{sd}. This apparent change of the parameter α, which can also take up the reversed order, is currently not understood.

V. SUMMARY

We have observed Fano resonances in CVD-grown SWNT's. The measured conductance evolves with reducing gate voltage from the single-electron tunneling regime at low coupling to the cotunneling regime at intermediate coupling. If the transparency to the contacts are increased further sharp resonances emerge superimposed on a weakly varying background. These resonances are identified as Fano resonances and can reasonably well be modeled with the traditional Fano approach of interference between a resonant and a nonresonant channel without interaction. The source of the two channels may reside in different tubes within one bundle, one weakly coupled to the contacts and the other strongly. This scenario is appealing because bundling is an ubiquitous phe-

nomenon in the growth process of carbon nanotubes. It also occurs in CVD-grown tubes, which are studied here. However, it is quite surprising that the measured electrical conductance is bound by $4e^2/h$, which is the maximum possible for a *single* nanotube. In case of the interference between two and more nanotubes one would expect the conductance to exceed this value for certain gate voltage values. We have pointed out, that Fano resonances may also arise intrinsically, even if the two orbital states are both strongly coupled to the contacts. Future work must clarify the role of intrinsic and extrinsic Fano resonances in SWNT's.

ACKNOWLEDGMENTS

We acknowledge fruitful discussions with W. Belzig, T. Kontos, and D. Loss. This work has been supported by COST and the RTN DIENOW (EU-5th framework), the Swiss NFS, and the NCCR on Nanoscience.

*Electronic address: Christian.Schoenenberger@unibas.ch

[1] J. O. Connerade and A. M. Lane, Rep. Prog. Phys. **51**, 1439 (1988).
[2] U. Fano, Phys. Rev. **124**, 1866 (1961).
[3] R. K. Adair, C. K. Bokelman, and R. E. Peterson, Phys. Rev. **76**, 308 (1949).
[4] J. A. Simpson and U. Fano, Phys. Rev. Lett. **11**, 158 (1963).
[5] F. Cerdeira, T. A. Fjeldly, and M. Cordona, Phys. Rev. B **8**, 4734 (1973).
[6] V. Madhavan, W. Chen, T. Jamneala, M. F. Crommie, and N. S. Wingreen, Science **280**, 567 (1998).
[7] J. Li, W. D. Schneider, R. Berndt, and B. Delley, Phys. Rev. Lett. **80**, 2893 (1998).
[8] J. Göres, D. Goldhaber-Gordon, S. Heemeyer, M. A. Kastner, H. Shtrikman, D. Mahalu, and U. Meirav, Phys. Rev. B **62**, 2188 (2000).
[9] K. Kobayashi, H. Aikawa, S. Katsumoto, and Y. Iye, Phys. Rev. Lett. **88**, 256806 (2002).
[10] K. Kobayashi, H. Aikawa, S. Katsumoto, and Y. Iye, Phys. Rev. B **68**, 235304 (2003).
[11] C. Fühner, U. F. Keyser, R. J. Haug, D. Reuter, and A. D. Wieck, Prog. Solid State Chem. **4**, 1305 (2003); C. Fühner, U. F. Keyser, R. J. Haug, D. Reuter, and A. D. Wieck, cond-mat/0307590 (unpublished).
[12] K. Kobayashi, H. Aikawa, A. Sano, S. Katsumoto, and Y. Iye, cond-mat/0311497 (unpublished); H. Aikawa, K. Kobayashi, A. Sano, S. Katsumoto, and Y. Iye, cond-mat/0312431 (unpublished).
[13] J. Kim, J. R. Kim, Jeong-O Lee, J. W. Park, H. M. So, N. Kim, K. Kang, K. H. Yoo, and J. J. Kim, Phys. Rev. Lett. **90**, 166403 (2003).
[14] W. Yi, L. Lu, H. Hu, Z. W. Pan, and S. S. Xie, Phys. Rev. Lett. **91**, 076801 (2003).
[15] Z. Zhang, V. Chandrasekhar, D. A. Dikin, and R. S. Ruoff, cond-mat/0311360 (unpublished).
[16] U. Fano, Nuovo Cimento **12**, 156 (1935).
[17] A. A. Clerk, X. Weintal, and P. W. Brouwer, Phys. Rev. Lett. **86**, 4636 (2001).
[18] A. Yacoby, M. Heiblum, D. Mahalu, and H. Shtrikman, Phys. Rev. Lett. **74**, 4047 (1995).
[19] M. Krüger, M. Buitelaar, T. Nussbaumer, L. Forró, and C. Schönenberger, Appl. Phys. Lett. **78**, 1291 (2001).
[20] M. R. Buitelaar, A. Bachtold, T. Nussbaumer, M. Iqbal, and C. Schönenberger, Phys. Rev. Lett. **88**, 156801 (2002).
[21] B. Babić, M. Iqbal, and C. Schönenberger, Nanotechnology **14**, 327 (2003).
[22] B. Babić, J. Fuhrer, M. Iqbal, and C. Schönenberger, *Proceedings of the XVIIIth International Winterschool on Electronic Properties of Novel Materials*, Kirchberg, 2004, edited by H. Kuzmany, J. Fink, M. Mehring, and S. Roth (AIP, New York, 2004).
[23] A. Javey, J. Guo, Q. Wang, M. Lundstrom, and Hongjie Dai, Nature (London) **424**, 654 (2003).
[24] R. Martel, V. Derycke, C. Lavoie, J. Appenzeller, K.K. Chan, J. Tersoff, and Ph. Avouris, Phys. Rev. Lett. **87**, 256805 (2001).
[25] D. Goldhaber-Gordon, H. Shtrikman, D. Mahalu, D. Abusch-Magder, U. Meirav, and M. A. Kastner, Nature (London) **391**, 156 (1998).
[26] Leo Kouwenhoven and Leonid Glazman, Phys. World **Jan**, 33 (2001).
[27] J. Nygård, D. Cobden, and P. E. Lindelof, Nature (London) **408**, 342 (2000).
[28] M. R. Buitelaar, A. Bachtold, T. Nussbaumer, M. Iqbal, and C. Schönenberger, Phys. Rev. Lett. **88**, 156801 (2002).
[29] Wenjie Liang, Marc Bockrath, and Hongkun Park, Phys. Rev. Lett. **88**, 126801 (2002).
[30] A detailed analysis of the Kondo effect, in particular the fundamental question on the nature of the ground state at half-filling will be published in a different paper, cond-mat/0407193 (unpublished).
[31] W. Liang, M. Bockrath, D. Bozovic, J. H. Hafner, M. Tinkham, and H. Park, Nature (London) **411**, 665 (2001).
[32] I. G. Zacharia, D. Goldhaber-Gordon, G. Granger, M. A. Kastner, Yu. B. Khavin, H. Shtrikman, D. Mahalu, and U. Meirav, Phys. Rev. B **64**, 155311 (2001).
[33] M. L. Ladrón de Guevara, F. Claro, and P. A. Orellana, Phys. Rev. B **67**, 195335 (2003).
[34] B. Kubala and J. König, Phys. Rev. B **65**, 245301 (2003).
[35] B. Kubala and J. König, Phys. Rev. B **67**, 205303 (2003).
[36] Yoseph Imry, *Introduction to Mesoscopic Physics* (Oxford University Press, New York, 1997).
[37] M. Bockrath, D. H. Cobden, A. G. Rinzler, R. E. Smalley, L. Balents, and P. L. McEuen, Nature (London) **397**, 598 (1999).
[38] M. Bockrath, D. H. Cobden, P. L. McEuen, N. G. Chopra, A. Zettl, A. Thess, and R. E. Smalley, Science **275**, 1922 (1997).
[39] P. L. McEuen, M. Bockrath, D. H. Cobden, Y. G. Yoon, and S. G. Louie, Phys. Rev. Lett. **83**, 5098 (1999).
[40] S. J. Tans, M. H. Devoret, H. Dai, A. Thess, R. E. Smalley, L. J. Geerligs, and C. Dekker, Nature (London) **386**, 474 (1997).
[41] B. Babić, J. Furer, S. Sahoo, S. Farhangfar, and C. Schönenberger, Nano Lett. **3**, 1577 (2003).